CWP-325
November 1999

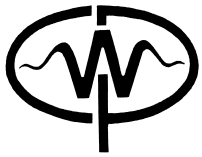

The Quality of the Surface-Consistency Assumption in Residual-Statics Estimation

Gabriel Perez* and Ken Larner†

*Ecopetrol-ICP, A.A 4185 Bucaramanga, Colombia;
formerly Colorado School of Mines

†Department of Geophysics and Center for Wave Phenomena,
Colorado School of Mines, Golden, CO 80401.

Center for Wave Phenomena
Colorado School of Mines
Golden, Colorado 80401
303/273-3557

ABSTRACT

Founded on the assumptions of surface consistency and time-invariance, reflection-based residual-statics estimation and correction addresses, from a statistical viewpoint, rapid near-surface variations that are beyond the resolution of alternative methods that aim to correct for time distortions in seismic data. These inter-related assumptions, however, strictly are founded on a simplistic, vertical-path model of wave propagation in the near-surface. Through a finite-difference modeling study, using near-surface models that are admittedly simple and idealized (homogeneous weathered layer with a sinusoidal base), we assess and draw general conclusions about the validity of the assumption of surface consistency in reflection data. As encountered in practice, the quality of the assumption degrades with increasing ratio of spreadlength to reflector depth. The validity of the surface-consistency assumption is best for longer-wavelength anomalies in a weathering layer that is relatively thin. Wavefront healing, however, limits seriousness of the time-distortion problem where the weathering layer is relatively thick. Interestingly, wavefront healing also helps reduce the size of the time-distortion problem when the velocity in the surface layer is large relative to that in the layers beneath, such as in areas of permafrost.

INTRODUCTION

Reflection data from land seismic surveys typically suffer from time distortions attributed to anomalies in the velocity and thickness of near-surface layers. Because near-surface layering can be viewed as a filter whose response depends on the path of the seismic wave, variations in surface elevation, and in near-surface thickness and velocity, introduce phase and amplitude distortion of the propagating wavefront (Taner *et al.*, 1974). Accurate estimation of this filter is difficult in practice, mainly because of the poor definition of near-surface structure provided by conventional seismic exploration techniques, which are aimed at deeper subsurface targets. Conventional methods aimed at correcting for near-surface-induced distortions avoid the complex problem of estimating the full wave-theoretical, near-surface filter response by making simplifying assumptions (Hileman *et al.*, 1968; Taner *et al.*, 1974; Wiggins *et al.*, 1976); corrections are estimated as simple time-invariant (i.e., static) time delays applied to the seismic traces. Furthermore, these are assumed to be "surface consistent;" that is, a single time delay is assigned to each particular source location and to each receiver-group location, regardless of the details of wave propagation (see Figure 1).

These assumptions, which allow us to approach the problem of correcting for the time distortions from a statistical viewpoint, are founded on the implicit assumption that travel paths for seismic energy through the near-surface are vertical; they also imply that wave-theoretical influences on time distortions can be ignored (Larner *et al.*, 1996). Vertical propagation is approximately correct if the velocity of the weathering layer is much lower than that in the sub-weathering and the bottom of

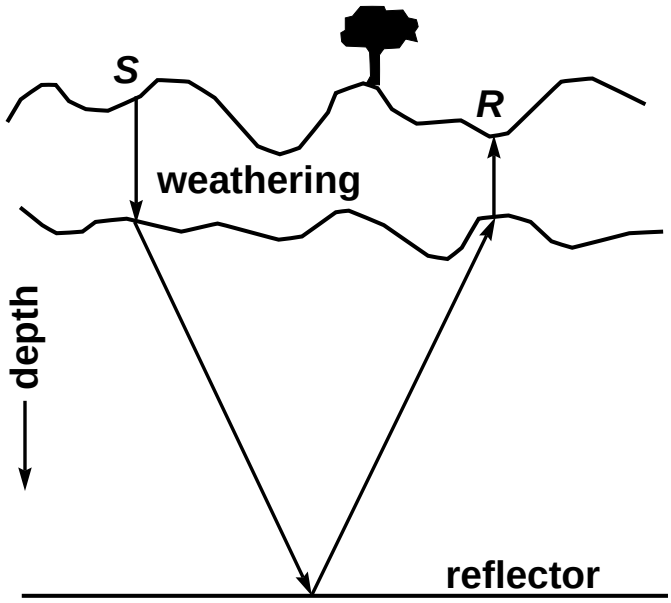

FIG. 1. Surface-consistent statics model: if waves propagated as vertical rays through the near-surface, time distortions would consist of a single time-invariant delay for each shot (S) and each receiver (R) position.

the layer is horizontal. Other factors often cited to favor the validity of the assumptions are (Marsden, 1993a) small source-to-receiver offsets, small surface-elevation changes, and a weathering layer that is relatively thin. It is clear how these factors influence the extent of departure from vertical travel path for a ray-theoretical model of propagation; not so clear, however, is how they relate to wave-theoretical aspects of the problem.

Even if static-estimation methods based on surface consistency yield robust and useful solutions most of the time in common practice, little has been understood about the magnitude of the errors incurred under that assumption. To examine the validity of the surface-consistency assumption, it would be good to generate somewhat "realistic" time distortions by some modeling procedure. Here, however, the question arises as to how to define a velocity model of the near-surface that is either sufficiently accurate or sufficiently representative so that the generated distortions resemble those found in field data. An alternative, which we follow here, is to choose simple, non-realistic models, characterized by a few key parameters, in hopes that clear and unambiguous relationships can be established between analysis results and model parameters.

The performance of different methods for static-correction estimation is highly dependent on the wavelength of different components of the solution. In particular, surface-consistent, reflection-based estimation techniques (so-called "residual-statics estimation methods") are capable of accurately solving for short-wavelength (relative to the receiver spreadlength) lateral variations of the near-surface, but perform

poorly in handling long-wavelength ones (Wiggins *et al.*, 1976). Refraction-based and tomographic methods, in contrast, are more suited to solve for long-wavelength components of the solution (Yilmaz, 1988; Marsden, 1993b). Our choice of depth models here has been guided by the fact that residual-statics estimation primarily targets relatively rapid variations in the near-surface.

MODELING WAVE-THEORETIC TIME DISTORTIONS

The near-surface model chosen for study

Even if a detailed, realistic model of the near-surface could be developed and studied, we would not trust that valid general conclusions could be drawn from the study results for specific models. We have thus pursued a different approach to defining a velocity model for our investigation into the surface-consistency assumption. We use simple models, characterized by just a few parameters, that feature short-wavelength lateral variations in the near-surface layer.

In their classic eigenvector analysis of residual-static corrections as a general linear inverse problem, Wiggins et al. (1976) were able to learn much about the quality of the statics solution as a function of spatial wavelength of the statics variations. Their analysis had the advantage that the surface-consistency assumption makes the problem a linear one. This, however, is not the case for our study of the quality of the surface-consistency assumption itself; differences between time distortions that honor the wave equation and those computed under the assumption of vertical raypaths through the weathering layer are nonlinearly related to the shape of the near-surface. Nevertheless, we believe that much can be learned about the quality of the surface-consistency assumption by considering models with sinusoidal lateral near-surface variations of differing wavelength.

To test that contention, we analyze wave-theoretic time distortions for plane reflectors in two-dimensional (2D) models whose near-surface layer structure is simply sinusoidal. As exemplified in Figure 2 and detailed in Figure 3, the general depth model in this study is characterized by a plane free-surface, a homogeneous weathering layer (velocity V_1) bounded below by a cosine-shaped interface (spatial wavelength D, amplitude h, and mean depth z_w), and a second homogeneous layer (velocity $V_2 =$ 2000 m/s) bounded at its base by a horizontal, plane interface (depth $Z = 1000$ m). A third layer (velocity $V_3 = 3000$ m/s), below this interface, completes the model. The model is 4500-m wide and 2000-m deep.

A typical test

In simulation tests on models with the geometry illustrated in Figures 2 and 3, we varied the parameters that define the sinusoidal base-of-weathering interface (i.e., the values of D, z_w and h). As in Figure 3, throughout this paper, we use the shorthand notation $D/z_w/h$ to characterize the choices of values for the three parameters; for

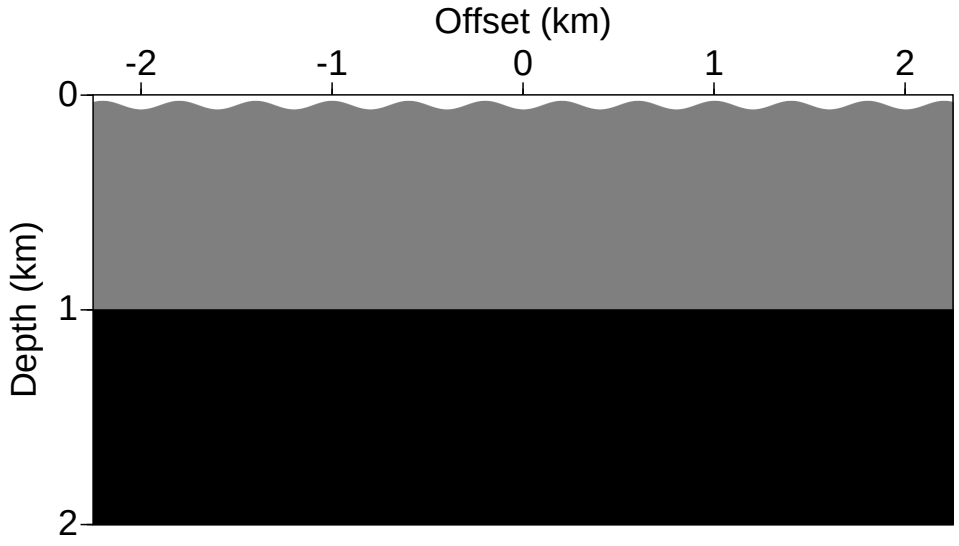

FIG. 2. Schematic depth section depicting our generic model, which consists of a sinusoidal base-of-weathering and a deep, horizontal reflector. Darker shading indicates higher velocity.

example, the model in which $D = 400$ m, $z_w = 25$ m, and $h = 20$ m is denoted by 400/25/20.

To honor requirements for accuracy in our wave-theoretic modeling, we used a finite-difference algorithm [the explicit, fourth-order in space and second-order in time, acoustic-wave-equation modeling code of Fei and Larner (1995)], with a sufficiently fine grid step-size so as to accurately represent the seismic wavelengths being considered. We selected a step-size of 2.5 m for most of the tests performed. Standard references (Alford *et al.*, 1974) give an accuracy requirement of at least 5.5 points per wavelength for the algorithm used; this step-size should be sufficiently fine for frequencies up to about 70 Hz (seismic wavelength $\lambda_1 \approx 14$ m in the weathered layer); the dominant frequency in most of our tests is 30 Hz. Use of such a fine grid ensures that observed time distortions can be attributed to wave propagation and are not influenced by numerical artifacts of the computational algorithms. Moreover, a fine grid is necessary in order that the sinusoidal shape of the base-of-weathering be accurately characterized. Accurate representation of the sinusoidal interface was furthered by assigning to each grid cell containing a segment of the interface a velocity value computed from a weighted average of the slownesses above and below the interface. The weights were based on the vertical distances from the interface to the grid points above and below. This is similar to the approach of Muir et al. (1992); more details are given in Perez (1997).

Standard stability requirements (Alford *et al.*, 1974) were met with the choice of a 0.5-ms time-step for wavefield updating. Each test involved the computation of a

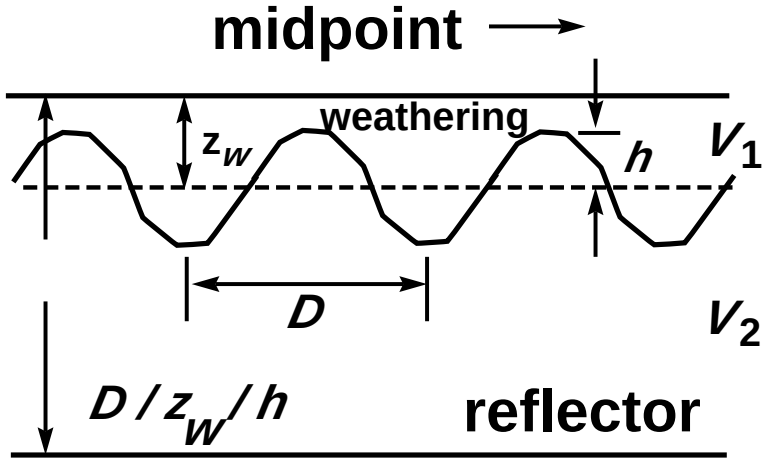

FIG. 3. Parameters describing the geometry of the depth models in the study. The notation $D/z_w/h$ will be used throughout the paper.

single shot record (the source signature was a symmetric, zero-phase Ricker wavelet), with source position centered on the upper boundary of the model, and receivers located every 2.5 m along that surface. Following the approach of Clayton and Engquist (1977), we implemented absorbing boundaries at the top, bottom, and side boundaries of the model. The choice of absorbing boundary at the top of the model may seem curious since the presence of surface-related multiples dramatically changes the appearance of the data as compared to the results obtained with the absorbing-boundary condition. Specifically, interference with surface-generated multiples alters the shape and frequency content of the wavelet in the data. In all our tests, however, we found that the character of the observed time distortions was comparable for both choices of top-boundary condition as long as the frequency content of the resulting wavelet was similar.

In a typical test, the modeled traces are 1.5-s long. Given the fine grid in space and time required for the modeling, calculation of a single shot record took about 70 minutes of CPU time running in a single processor on a Silicon Graphics Power Challenge computer with 256-Mb total memory. Further discussion on the details of the modeling experiments, the representation of the sinusoidal base-of-weathering interface, and the choice of a boundary condition at the top boundary of the model are given in Perez (1997).

A LOOK AT THE DATA

Figure 4 shows a representative shot record for a test with a 400-m wavelength base-of-weathering. This value of D is much larger than the dominant seismic wave-

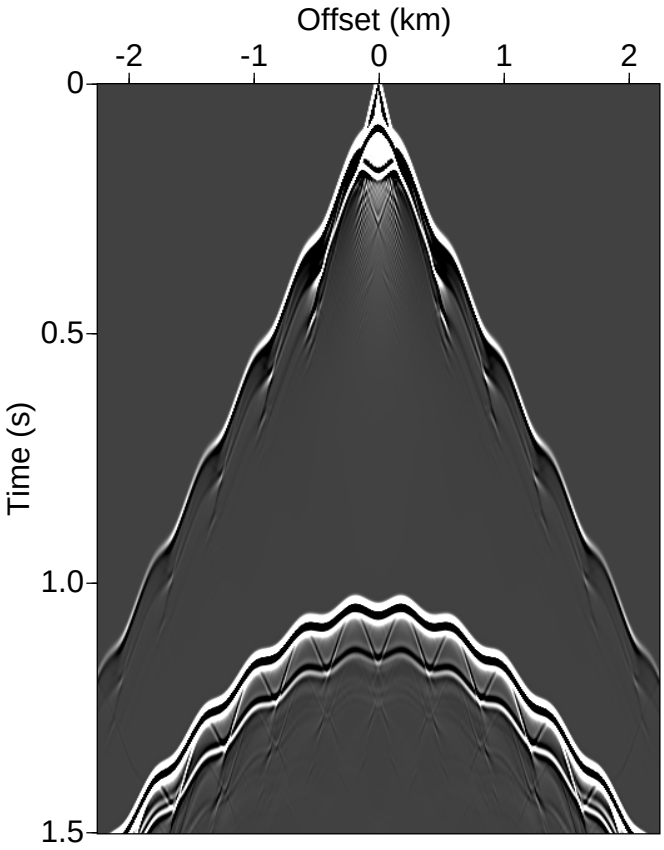

FIG. 4. Synthetic shot record generated for a depth model as illustrated in Figure 2, with a $D = 400$ m, $z_w = 25$ m, $h = 20$ m geometry for the sinusoidal base-of-weathering. The source signature was a Ricker-wavelet with 30-Hz peak frequency. Several events can be observed: the refraction first-arrival from the corrugated base-of-weathering; the reflection from that interface, arriving later than the first-arrivals and becoming quite weak past about a 0.5-km offset; the time-distorted reflection from the deep horizontal reflector, with apex just below 1.0 s. A weaker, but still visible source-related multiple (some 0.1 s later than the primary reflection), as well as weak receiver-related multiples (the large-moveout events visible between the primary and the source-related multiple), evidence imperfections in the performance of the absorbing boundary at the top surface of the model.

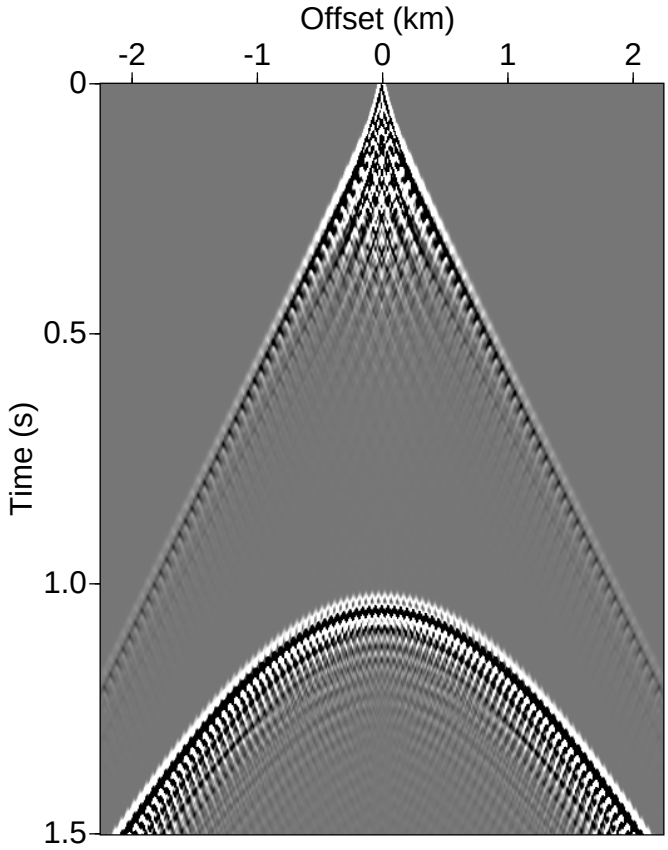

FIG. 5. Synthetic shot record generated for the 50/25/20 model. Observe the complex mixture of interfering reflection and diffraction events following both the first arrivals and the deep reflection. These events are related to the presence of a short-wavelength corrugated base-of-weathering.

length in the weathered layer, but it is still considered a short-wavelength anomaly from the perspective of residual-statics estimation (Wiggins et al., 1976). The time distortions of interest in the course of this work are exemplified in Figure 4 by the oscillating departures in reflection time from the nearly hyperbolic moveout that would be observed if the base-of-weathering were flat.

For comparison, Figure 5 shows the shot record generated for a model with a shorter wavelength, $D = 50$ m, other parameters unchanged from those for Figure 4. Note that a 25-m group interval, which is common in current seismic-acquisition practice, would sample the 50-m-wavelength anomaly at Nyquist wavenumber. Thus, this could be considered a "very" short-wavelength anomaly. Examination reveals time distortions in the primary deep reflection, but these are much smaller than those observed in Figure 4. This is an example of the general behavior that a reduction in D, where other parameters are unchanged, introduces both relatively strong diffractions from the sinusoidal base-of-weathering and a reduction in the amplitude of the time distortions.

Though the shot records are not shown here, we performed tests to compare the results of the finite-difference modeling with those from a ray-tracing modeling program. For values of D as small as 100 m, ray-tracing results reproduced the finite-difference data with acceptable accuracy, but the modeled data differed substantially for smaller values of D. A rule-of-thumb for the validity of ray theory is that the scale-length of a problem must be at least three times as large as the seismic wavelength (Bleistein, 1984). That is indeed the case when $D \geq 100$ m, for the 30-Hz dominant frequency, for which the seismic wavelength in the near-surface layer in our tests is 33 m.

TIME DISTORTIONS IN THE SYNTHETIC DATA

We compute quantitative values for the time distortions in our test data by cross-correlation of the generated data with a reference shot record. That reference is obtained for a model in which the sinusoidal interface has been replaced by a horizontal one at the mean depth z_w of the corrugated interface (i.e., one for which $h = 0$). For each trace, we compute the crosscorrelation over a narrow window centered on the deep reflection of interest and then pick the time-lag of the maximum cross-correlation value. This picked time-lag is our measure of the relative time distortion induced by the presence of the corrugated base-of-weathering.

Time distortions for all the tests that we performed exhibit features similar to those in the curves shown in Figures 6 through 10. For comparison in those and similar figures throughout the paper, the dashed lines show the time distortions computed simplistically as vertical-path receiver statics (i.e, computed as the difference in vertical traveltime between the sinusoidal and horizontal base-of-weathering models, at receiver locations). This procedure is equivalent to subtracting the vertical-path shot static (which is computed in a way similar to that for receiver-statics, but at the shot location) from the total static (the sum of shot-plus-receiver static). The magnitude of the vertical shot static is also subtracted from the raw picked time-lags (i.e., the time-lag values obtained by the crosscorrelation and picking procedure described above). When the shot static is close to the mean value of the raw picked time-lags, the solid curve in the time-distortion plots has approximately zero mean. That is not the case when the time distortions in the data depart significantly from the vertical-path statics (such as in Figure 7, below).

When D is large compared to the seismic wavelength (as in Figure 6), the time distortions are similar to the vertical-path statics (the solid and dashed curves are close to one another), with differences growing mildly with increasing offset. As noted above, large D defines the regime in which ray theory is valid. Indeed the increasing departure of the two curves with increasing offset is not attributable to any shortcoming in the ray theory, but, rather, to the simplistic use of vertical paths in the computation of surface-consistent statics. Raypaths depart from vertical in the near-surface, increasingly for increasing offsets. Moreover, the departure between computed time distortions and vertical-path statics is larger for the peaks than for the

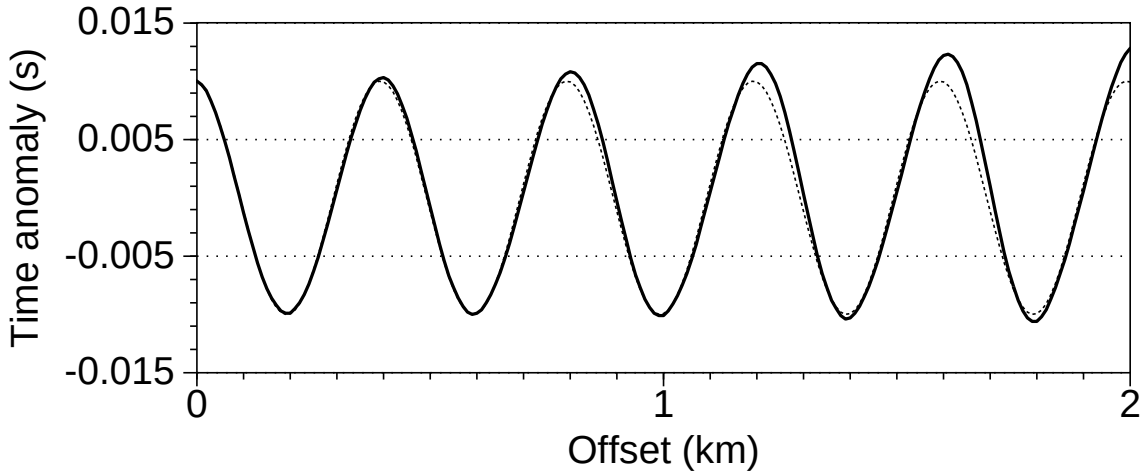

FIG. 6. Solid line: wave-theoretic time distortions estimated for the reflection in Figure 4. Dashed line: corresponding surface-consistent (vertical-path) receiver statics. This convention is followed in similar plots throughout the paper. The wavelet used to generate the shot record for this test and for those in the following four figures is Ricker with a 30-Hz peak frequency. Only the distortions for positive source-to-receiver offset are shown since the distortions are symmetric with offset.

troughs in the time-distortion curve in Figure 6 (e.g., the greater difference between the solid and dashed lines around a 1.6-km offset, compared to that at 1.8 km). This is due to the difference in the length of the slant raypath through the low-velocity, weathered layer as the ray emerges from different positions along the sinusoidal interface: this length is largest for a ray emerging from a trough (where the weathering layer is thickest) and smallest for one emerging where it is most thin.

Figure 7 exhibits a characteristic quite different from that seen in Figure 6. For Figure 7, the model has a smaller $D = 50$ m, but maintains the ratio $D/h = 20$, as well as the depth $z_w = 25$ m. The magnitude (defined as half the peak-to-trough amplitude of the oscillations) of the computed time distortions is much smaller than that of the vertical statics, decreasing with increasing offset. A "wavefront healing" phenomenon is present in this case, with action that becomes stronger for increasing offset. Such wave-theoretical phenomena become important as the seismic wavelength becomes large compared to the wavelength D of the corrugated base-of-weathering. Also observed in the time distortions of Figure 7 is an overall negative shift in the mean value of the distortions. We discuss this behavior below.

In Figure 8, the amplitude h of the sinusoidal base-of-weathering has increased to 20 m, compared to 2.5 m in Figure 7. Again, the amplitude of the computed time distortions is reduced relative to that of the corresponding vertical-path statics, for offsets up to about 1.0 km. For larger offsets, the size of the measured distortions increases abruptly, and the distortion pattern departs significantly from being sinusoidal. Examination of the corresponding shot record (not shown here) revealed that it contained a strong level of diffracted and scattered events, which can be attributed

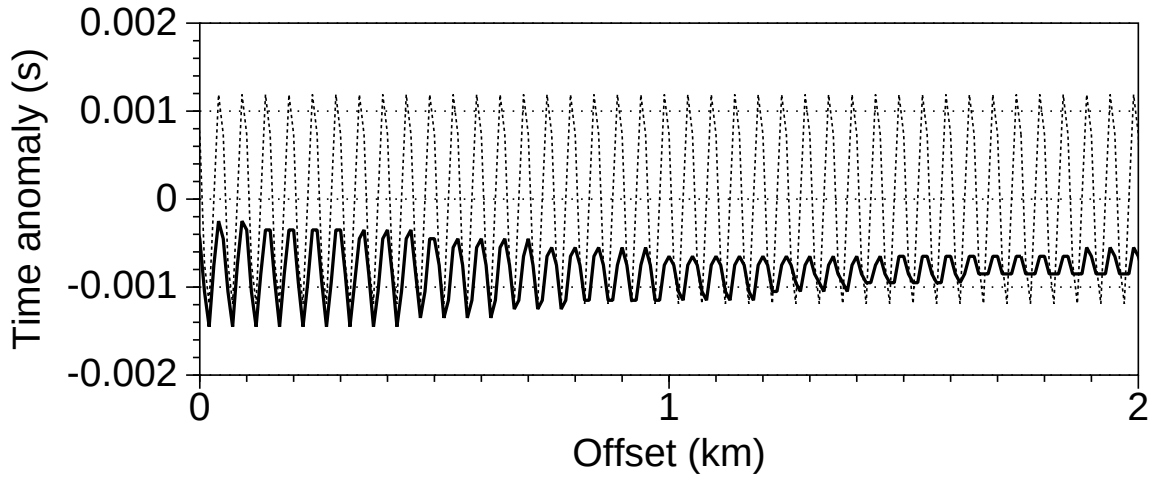

FIG. 7. Time distortions estimated for the data from the 50/25/2.5 model.

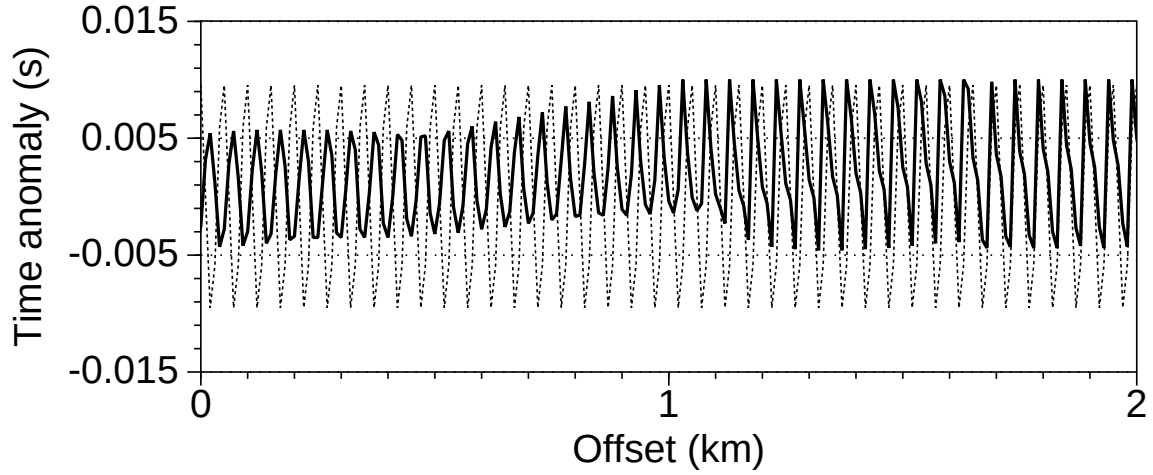

FIG. 8. Time distortions estimated for the data from the 50/25/20 model.

to the relatively large value of the ratio h/D. These events cause a departure of the peaks of autocorrelation lags from those associated with the desired primary reflections. The strict constructive interference of the regular pattern of diffractions caused by the periodicity of the corrugations in that interface is a shortcoming of our sinusoidal model for large h/D.

In Figure 9, the depth of the base-of-weathering has been increased relative to that for Figure 8, to $z_w = 50$ m, yielding a general reduction in the magnitude of the distortions relative to that of the vertical-path statics, but little variation in that magnitude with offset. Note that near zero-offset the phase of the time distortions is opposite that of the vertical-path statics. The phase changes gradually with offset, so that the phases match fortuitously beyond about 1.5-km offset. A similar behavior is observed in Figure 8. Also observed in Figures 8 and 9 is a drift in the mean value of the time distortions toward higher values for the longer offsets compared to those

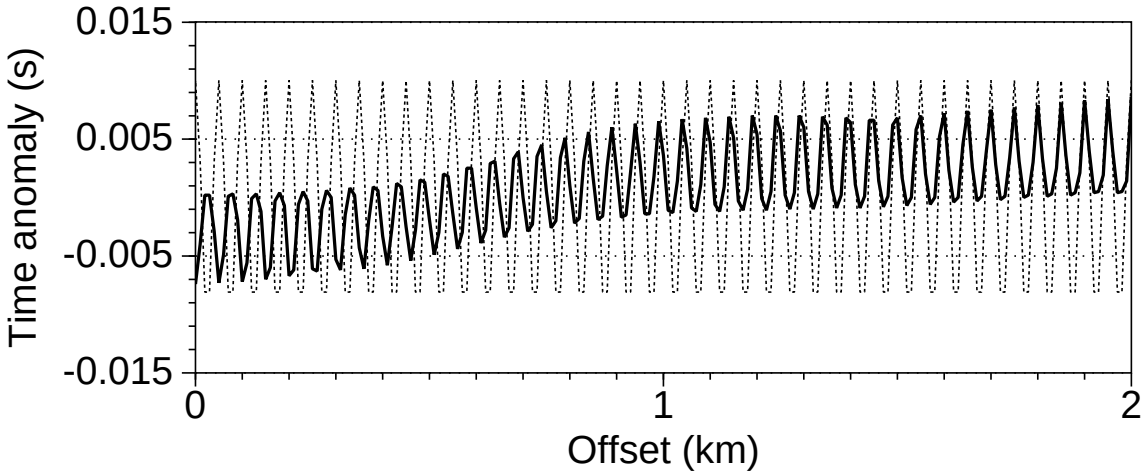

FIG. 9. Time distortions estimated for the data from the 50/50/20 model.

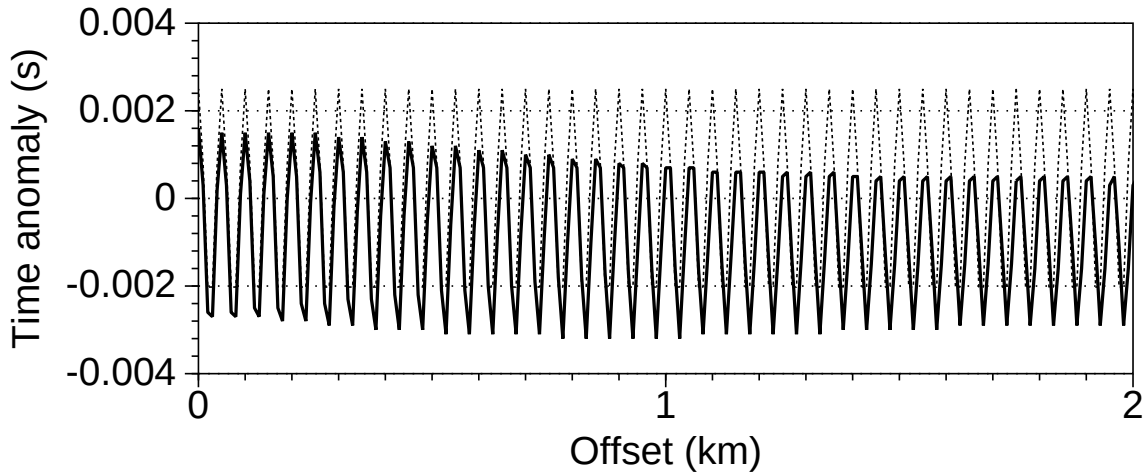

FIG. 10. Time distortions estimated for the data from the 50/10/5 model.

near zero-offset.

Finally, in Figure 10, the average thickness of the weathering layer has been reduced to $z_w = 10$ m. Only a relatively small reduction in the overall size of the distortions is observed here, and the variation in the magnitude of the distortions with increasing offset is also rather small; wavefront healing has been reduced as a result of the decrease in the mean thickness of the weathering.

THE CHARACTER OF THE TIME DISTORTIONS

The Fresnel zone concept

By Huygens's principle, a finite portion of a reflector contributes to the reflection seen in a seismic trace, the size of which is usually estimated using the concept of

a *Fresnel zone* (Sheriff, 1980; Berkhout, 1984). The Fresnel zone may be defined as the portion of a reflector from which reflected energy reaches a receiver within a sufficiently short time after the first reflection arrival such that contributions from this zone add constructively to produce the observed reflection. The maximum delay time is usually set as a fraction of the period of the seismic wave: common choices are half a period (Sheriff, 1980) and a quarter of a period (Berkhout, 1984). The three-dimensional generalization of the concept of Fresnel zone is a *Fresnel volume* (Cerveny & Soares, 1992). As illustrated in Figure 11, the Fresnel volume for a given event, such as the reflection from the deep interface in our modeling experiments, is the locus of scattered-energy paths from points on the reflector such that the sum of traveltimes from the point to the source and from the point to the receiver is within some small delay time of the specular reflection time from the source to the receiver, so that contributions from these paths interfere constructively. Červený and Soares (1992) show that, in a homogeneous medium, the shape of the Fresnel volume is that of an ellipsoid whose foci are coincident with the source and receiver locations. Wave propagation can be thought of as a spatial convolutional process that smears information from a finite portion of the medium, and the Fresnel volume is an estimate of the region of the medium effectively contributing in that process.

As illustrated in Figure 11, we can think of a Fresnel zone on a reflector as the intersection of the interface with the Fresnel volume for the primary reflection of interest. Likewise, the Fresnel zone on the *base-of-weathering* for the deep reflection in our tests represents the portion of the base-of-weathering that contributes energy to the deep reflection, and hence to the character and magnitude of the observed time distortions.

To estimate the width F of that "contributing portion" of the base-of-weathering, refer to Figure 12, where, for simplicity, we consider a zero-offset situation. Depicted in the figure is an ellipse that is defined by points P such that the sum of the traveltimes from any point P to the source location S and to the receiver location R exceeds the time of the direct arrival from S to R by a quarter of a period. For a homogeneous medium (otherwise the points P would define a boundary that is no longer elliptical), this condition fits the geometrical relation

$$\sqrt{z_w^2 + F^2/4} + \sqrt{F^2/4 + (2Z - z_w)^2} - 2Z = \lambda/4, \tag{1}$$

from which algebraic manipulation leads to equation (2). Here, λ is the seismic wavelength.

For our models, in which the seismic wavelength is not small relative to the average thickness of the weathering layer, the width F of the contributing zone along the base-of-weathering (beneath either the source or the receiver), as depicted in Figure 12, is given by

$$F = \frac{0.25\ \sqrt{\lambda_1\ (\lambda_1 + 16Z)\ (\lambda_1 + 16Z - 8z_w)\ (\lambda_1 + 8z_w)}}{\lambda_1 + 8Z}\ , \tag{2}$$

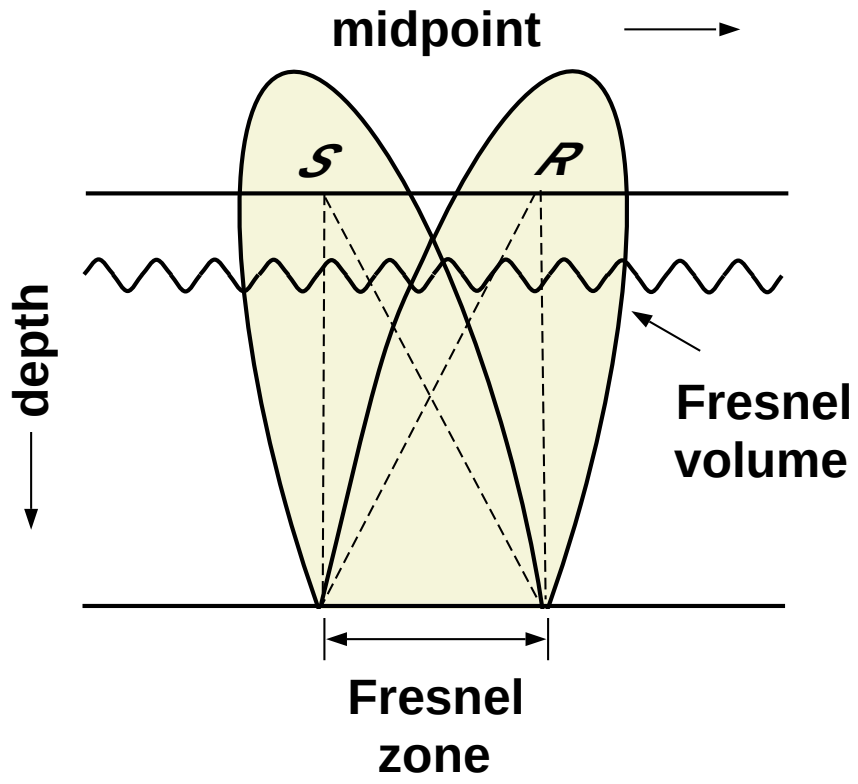

FIG. 11. Schematic cross-section through the Fresnel volume for a reflection from the deep interface in our model. Portions of waves traveling within the Fresnel volume will contribute constructively to a single observed reflection. The intersection of an interface and the Fresnel volume determines the Fresnel zone for that interface. One can then refer to a separate Fresnel zone in the deep interface and another in the base-of-weathering. (The Fresnel volume is strictly ellipsoidal, as depicted here, only for the special case of a homogeneous medium, including the region above the free-surface.)

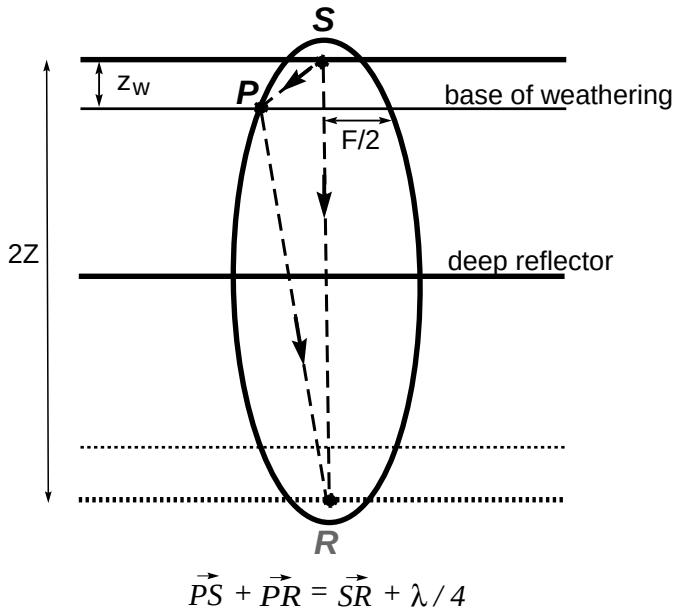

FIG. 12. Geometry used to estimate the width of the portion of the base-of-weathering contributing to a reflection arrival, using the concept of Fresnel zone, for a coincident source and receiver. The receiver is shown as the image of the source with respect to the reflecting interface at depth Z.

where $\lambda_1 = V_1/f$ is the seismic wavelength in the weathered layer, f is dominant frequency, Z is the depth of the reflector whose reflection contains the time distortions, and z_w is again the mean depth of the base-of-weathering. As seen below, equation (2) helps in understanding the behavior of time distortions in our test results.

The contributions to the composite output from different points along the extent of the contributing zone are not equally weighted, however. Greater contribution would come from the central portion of the zone, compared to that from the outer portions (Berkhout, 1984; Snieder & Lomax, 1996) because a larger relative number of raypaths that satisfy the quarter-wavelength criterion pass through that central region. Therefore, we can expect the *effective* size of the contributing zone to be smaller than that predicted by equation (2), increasingly so for near-field situations (e.g., for small z_w), where seismic amplitude varies inversely with the square of the distance from the source. Clearly, the size of the contributing zone is frequency-dependent, being larger as frequency decreases. We shall use the peak frequency in the source wavelet as an estimate of the dominant frequency in the data.

Dependence of the amplitude of time distortions on the size of the contributing zone

We can expect that the time distortions of interest here are influenced by the width along the corrugated boundary over which Huygens secondary sources contribute constructively to the dominant frequency component in the observed reflec-

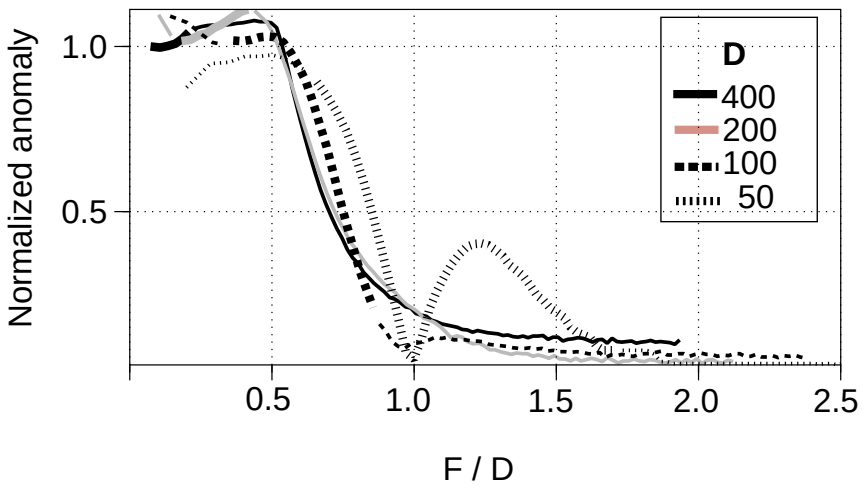

FIG. 13. Normalized anomaly (ratio of the magnitude of the time distortions, from the finite-difference modeling, to the corresponding vertical-path statics) as a function of the ratio of the width F of the contributing zone to the wavelength D of the base-of-weathering. Magnitude is estimated as the root-mean-square (rms) peak-to-trough amplitude of the time distortion measured in a 1.0-km window centered around zero-offset.The thick-line portion of each curve (as well as those in the next two figures) indicates values for the frequency range from 10 to 50 Hz, common in field data; this more reliable portion is small in the curves for $D = 400$ m and $D = 200$ m, restricted to low values of the ratio F/D. Note that F/D increases with decreasing frequency. Each curve was computed for a different value of D, keeping $D/h = 20$ and $z_w = 25$ m.

tion. Therefore, in our studies of the time distortions as a function of the model parameters D, h and z_w, we varied the dominant frequency in the data to sample a range of values of the width F. In each case, we computed the ratio of the magnitude of the time distortions to that of the corresponding vertical-path statics in a region near zero-offset, as a function of the ratio F/D, with F given by equation (2). We call this relative amplitude the "normalized anomaly."

Consider, first, variations in D. Figure 13 shows the normalized anomaly for D ranging from 400 m to 50 m, with a fixed ratio $D/h = 20$. Here, and in Figures 14 and 15, below, the thick-line portion of the curves highlights results for the range of frequencies between 10 and 50 Hz. The normalized anomalies plotted in these figures are unreliable for frequencies above about 50 Hz (i.e., small F/D) because of numerical dispersion in the finite-difference-generated data. Likewise, seismic data have little energy below 10 Hz, so results for large values of F/D cannot be trusted.

The curves in Figure 13 show a marked high-cut behavior in the normalized anomaly as a function of the ratio F/D. Differences among the curves in Figure 13 highlight that the time-distortion problem is indeed nonlinear. Those differences, however, are small for some of the curves, indicating that, for a range of values of D, the nonlinearity is not significant and that our definition of contributing region F is an acceptable one. The largest departure is observed for the smaller values of D (e.g.,

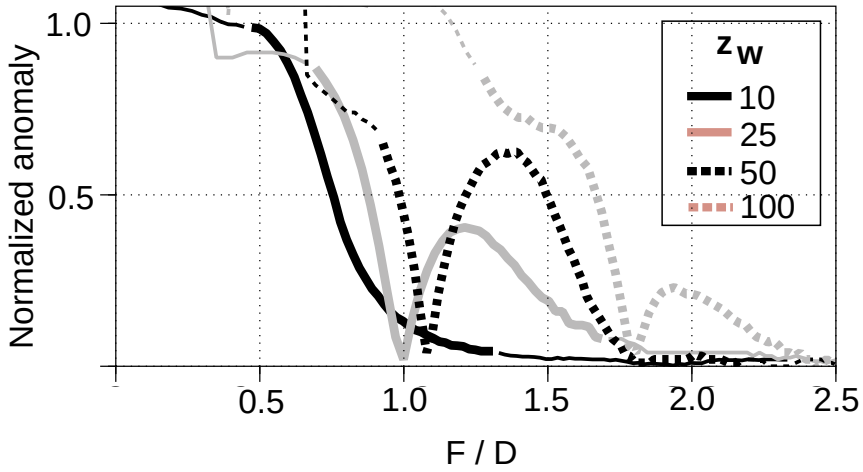

FIG. 14. Normalized anomaly as a function of the ratio F/D for tests in which z_w takes on several values ranging from 10 m to 100 m, while $D = 50$ m and $h = 5$ m. Again, the size of the distortions was estimated from an rms average of peak-to-trough time distortions near zero-offset.

the curve for $D = 50$ m). After having reached a minimum near $F/D = 1$, the curve for $D = 50$ m shows a "bounce back" to a cycle of increase and subsequent decrease in the size of the distortions with increasing F/D. Discussion of this behavior is given below.

Figure 14 shows normalized anomaly versus F/D for variations in the thickness z_w of the weathering. In contrast to Figure 13, the curves for different values of z_w here do not parallel each other so closely, although similarities exist in the general high-cut-filter trend for some of the curves. Time distortions behave in a highly nonlinear fashion as a function of z_w; the nonlinearity is higher for the larger values of z_w (e.g., the curve for $z_w = 100$ m exhibits the largest departure from the other curves). Again, the curves show a general trend of reduction in the relative size of the distortions with increasing values of F/D; in this case, however, several of the curves exhibit the bouncing back in the magnitude of the distortions past $F/D = 1$. Differences in the details of this bounce-back feature constitute a large part of the observed departures among the curves in Figure 14.

Finally, Figure 15 shows the results for variation in the amplitude h of the sinusoidal base-of-weathering. For small h, the magnitude of the time distortions is approximately independent of h, suggesting approximate linearity in the process that yields the time distortions. For relatively large values of h, scattering from the corrugated interface becomes important, contaminating estimates of time distortion and thus making the problem highly nonlinear. The results in Figure 15 suggest that $h/D \leq 0.1$ might be a criterion for defining what we could call small h. In Figures 14 and 15, the thick-line portion of the curves (pertaining to the range of frequencies considered of interest here) is generally within the high-cut region of F/D (i.e., normalized anomaly less than 1.0). Also in Figures 14 and 15, some of the curves (e.g.,

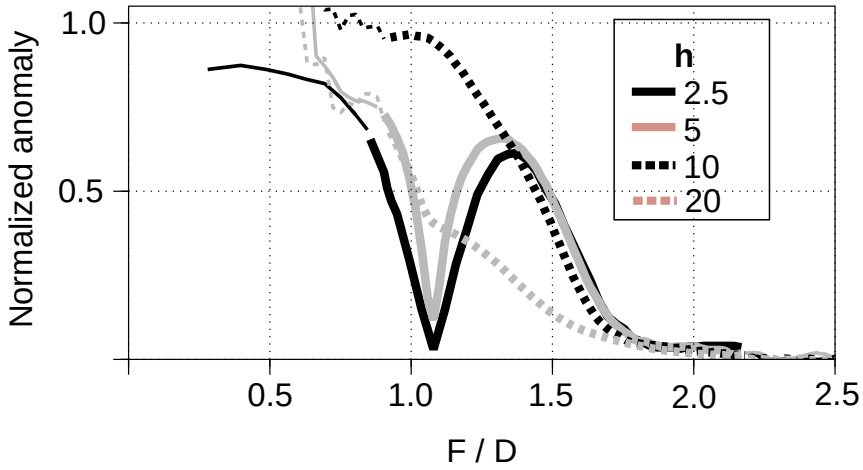

FIG. 15. Normalized anomaly versus F/D for different values of h, the height of the sinusoidal shape of the base-of-weathering. Here $D = 50$ m, $z_w = 50$ m, and h ranges from 2.5 m to 10 m.

those for $z_w = 50$ m and $z_w = 100$ m in Figure 14) exhibit an anomalous behavior for high frequencies (that is, small values of F/D), an artifact of numerical dispersion in the modeled shot-record data.

Discussion: dependence of time-distortion behavior on subsurface parameters

The behavior of the time distortions can be understood in terms of the distinction between ray- and wave-theoretical modeling of wave propagation. For sufficiently small values of F/D, the wavelength λ_1 in the weathering layer is also generally small relative to D, so results are in the high-frequency domain of validity of ray theory (Figures 13 through 15 suggest that $F/D < 0.5$ would be an adequate rule-of-thumb for defining a sufficiently small value of F/D for ray theory to be acceptable). For the region near zero-offset used to estimate the magnitude of the distortions in Figures 13 through 15, wave propagation is nearly vertical. If wave propagation in the near-surface can be validly described in terms of vertical-path propagation, the time distortions can be estimated as simple vertical-path statics, i.e., normalized anomaly close to 1.

As suggested above, since wave propagation involves contributions from a finite portion of the medium, the time distortions of interest in this work should be some average of the contributions from each point on the sinusoidal-shape interface, over the length of the contributing zone (Vasco *et al.*, 1995; Snieder & Lomax, 1996). As the width of the contributing zone increases, this averaging would smooth the observed time distortions compared to the time anomalies that would be obtained from simple ray theory, which, for zero-offset, would be conventional statics. As a result, when the wavelength D of the base-of-weathering is small compared with the size F of the region contributing to the recorded wavefield, the seismic waves perceive

little of the presence of lateral variations in the near-surface layer.

The width of the contributing zone decreases as the depth z_w decreases; moreover, as suggested above, equation (2) overestimates the size of the zone for small z_w, due to downweighting of contributions from outer portions of the zone in the near field. The smaller the contributing zone, the less smoothing of the time distortions due to averaging along the width of that zone. Therefore, for a given wavelength of near-surface variation and seismic frequency, we should not expect a significant decrease in the magnitude of the time distortions when the weathering layer is relatively thin. In his study of models for which an analytical solution of the wave equation is available, Combee (1994; 1995) has shown that the amplitude of wave-theoretical time distortions is not reduced much when the weathering thickness approaches zero. Taner et al. (1998) discuss a similar dependence on the weathering thickness for time distortions observed in refraction (first-break) arrivals.

The reduction in the amplitude of time distortions observed in our study occurs because of the oscillatory shape of the base-of-weathering. For a contributing zone larger than some threshold value (close to $F = D/2$), time distortions of opposite sign contribute to the averaging process, thereby lowering the magnitude of the average distortions. As seen in most of the curves in Figures 13 through 15, when the width of the contributing zone is close to D, the average yields small time distortion values, basically because the mean value of a sine function over a period is zero.

Consistent with this understanding of the time distortions as an average of sinusoidally-varying contributions, one would expect the time distortions to grow in magnitude (with opposite sign) past $F/D = 1$, reducing to low values again for $F/D = 2$, and so on. This characteristic, which we earlier referred to as a bounce-back of the normalized anomaly past $F/D = 1$, is observed in some, but not all, of the curves in Figures 13 through 15.

For reasons given earlier, this averaging process is not uniformly weighted along the width of the contributing zone. Outer portions of that zone contribute relatively less to the wavefield than does the central portion, particularly when z_w is small. This may explain the absence of the bounce-back in the normalized anomaly for $F/D > 1$ and small z_w. The absence of the regrowth past $F/D = 1$ for $z_w = 10$ m suggests that the effective width of the contributing zone is reduced to less than the width F described by equation (1). From the near-field argument above, one would then expect the absence of the regrowth when the near-surface layer is relatively thin, or, equivalently, when F/z_w is relatively large. In fact, we observe in Figure 13 that the regrowth is present only for the curve with $D = 50$ m, the case with the smallest ratio F/z_w. (Since z_w is fixed here, for $F/D \approx 1$, F/z_w is small when D is small.) In Figure 14, for only the smallest value of z_w is the regrowth absent. This dependence of the shape of these curves on F/z_w is further evidence of the nonlinearity in the problem of reflection time distortions.

If the observed time distortions result from some averaging of contributions from points along the sinusoidal base-of-weathering, then the net distortion should have

negative amplitude for, approximately, $1 < F/D < 2$ (i.e., the mean value of a sinusoidal function of wavelength D has negative amplitude for an averaging length roughly between D and $2D$). This would explain the observed difference between the phase of the time anomalies and that of the vertical-path statics seen in Figures 8 and 9, especially near zero-offset. For instance, from equation (2) the estimated width F of the contributing zone is 60 m (slightly larger than the corresponding $D = 50$ m) for the data in Figure 9.

So, the regrowth and sign change in the time distortions for F/D roughly between 1 and 2 corresponds to a second cycle of variation in the averaging process. Moreover, in the normalized-anomaly curves for the experiment with $z_w = 100$ m in Figure 14 (time-anomaly curves not shown here) the regrowth for $F/D > 1.8$ corresponds to a second bounce since the polarity of the time distortions returns to being positive for that bounce. The fact that the regrowth does not occur at $F/D = 2.0$, as might be expected, is indicative of the imperfect and qualitative nature of our understanding of the time distortions. Although the first bounce, which should occur for values of F/D between about 1.0 and 1.8, is not observed, results in this region are untrustworthy, largely because they are measured for relatively high frequencies, for which the modeled shot-record data are contaminated by dispersion.

The drift in the mean value of the distortions from near zero-offset to the longer offsets in Figures 7 through 10 can be attributed to variations in the contribution to the time distortions from near the shot: the *shot-associated* contributing zone in Figure 11 samples a changing region of the sinusoid as the receiver offset increases. In the common-shot configuration used for our tests, the portion of the contributing zone associated with the shot changes more slowly with offset than does that associated with the receiver. Therefore, the shot-related drift changes slowly with offset while the more rapid variations in the time distortions are attributable to variations in the contribution from the receivers.

For the smaller values of D, the time distortions have smaller magnitude than do the vertical-path receiver-statics. This leads us to expect the shot-associated contribution to the time distortion to be smaller than the vertical-path shot static, when D is small. Then, the mean value of the raw picks will be smaller than the vertical-path shot-static, and, as observed in Figure 7, subtraction of the shot-static from the raw picks of correlation lag yields quantities that, as opposed to the situation for relatively large D, are shifted toward negative values. A similar behavior is observed in Figures 9 and 10 near zero-offset. For longer offsets the situation is complicated by the drift. In contrast, the behavior at long offsets in Figure 8 is erratic because correlation lags for that test are contaminated by the strong diffractions and scattered events.

The wave-theoretical results discussed here indicate that we can expect to find significant near-surface-induced time distortions of a relatively short wavelength in field seismic data only when the thickness of the weathering is small. If short-wavelength distortions are observed, they either may be some sort of noise not associated with

near-surface anomalies or must have a shallow origin. Below, however, we find that although the time distortions that are associated with thicker weathering have relatively small amplitude, these are the ones that suffer most from failure of the surface-consistency assumption.

THE DEPARTURE FROM SURFACE CONSISTENCY

Even though the phenomenon may be interesting, the reduction in magnitude of the wave-theoretic time distortions for relatively short-wavelength lateral variations in the base-of-weathering is itself not a shortcoming of the assumption of surface consistency. For the sinusoidal base-of-weathering, surface consistency would imply a repetition of the sinusoidal pattern of time distortions for all offsets; it is the *departure from this pattern* that constitutes a failure of the assumption. Such a departure with offset is seen to varying extent in the wave-theoretical distortions, as exemplified by Figures 6 through 10.

To quantify the departure of the wave-theoretic time distortions from surface consistency, we shall generate sets of "*reference* surface-consistent time distortions" and then compute some measure of the difference between the reference time distortions and those obtained by the finite-difference modeling for our various near-surface models. Vertical-path statics (such as those in solid line in Figure 7), which are not obtained from wave theory, but instead consider only simple vertical-ray propagation in the near-surface model, typically would not serve as a useful reference. For example, when the sinusoidal base-of-weathering is relatively deep and has relatively short wavelength D, those vertical-path statics have considerably larger magnitude than do the wave-theoretic time distortions.

We postulate that an appropriate choice for the magnitude of the reference surface-consistent time distortions (let's call them "reference receiver statics" for short) is the rms average of the magnitude of the wave-theoretical time distortions over the offset range from 0 to some spreadlength X_{max}. We then take the shape of the reference receiver statics to be sinusoidal with offset (and, therefore, have magnitude and phase that are offset-invariant), with magnitude given by this average. We make the further assumption that receiver- and shot-statics are independent of one another, so that receiver statics can be explored without concern for the potential influence of shot-associated contributions.

Quantifying the departure from surface consistency

We will define errors in residual-statics estimation due to departure from the surface-consistency assumption as the difference between the wave-theoretical time distortions (modified as described in the next paragraph) and the sinusoidal reference receiver statics — for example, the difference between the solid- and dashed-line curves in Figure 16, for the 50/25/2.5 experiment with a spreadlength $X_{max} = 2.0$ km. The difference is plotted in Figure 17.

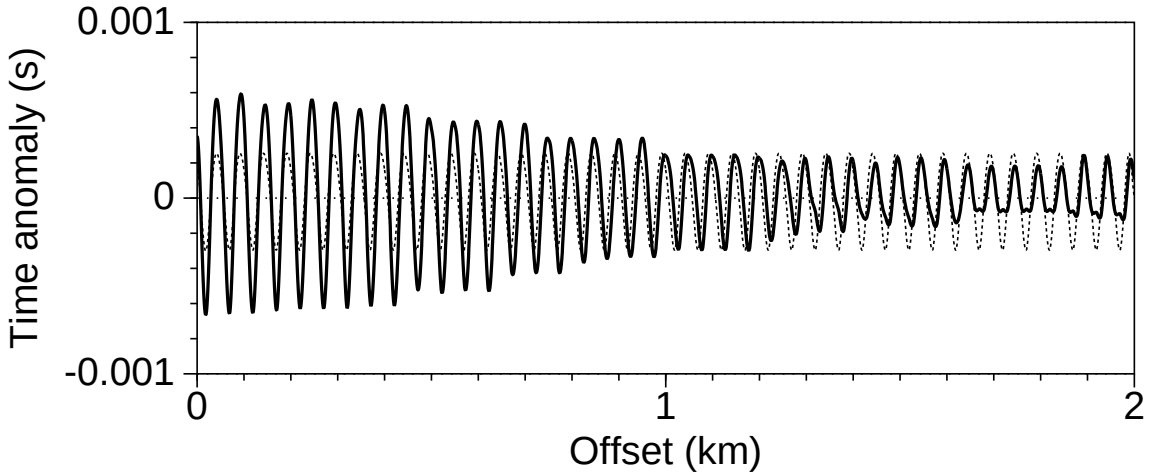

FIG. 16. Dashed curve: shape of the reference surface-consistent receiver statics, for the spreadlength X_{max} = 2.0 km in the 50/25/2.5 model. Solid curve: wave-theoretical time distortions, modified from those in Figure 7, as described in the text. Half the peak-to-trough height of the dashed-curve was set at the rms average of the magnitude of the time distortions between the offsets 0 and 2.0 km. Strict repetition with offset of the sinusoidal pattern is the defining behavior for surface consistency for the sinusoidal base-of-weathering model.

The solid curve in Figure 16 was obtained by subtracting the mean value (i.e., the DC component) and a long-wavelength trend (drift having wavelength larger than 1.0 km) from the time distortions estimated for the 50/25/2.5 experiment, the solid curve shown in Figure 7. Time-distortions preconditioned in this way constitute the input data for the estimation of errors associated with the departure from surface consistency for this and other experiments.

This preconditioning operation removes the (long-wavelength) drift in the mean value of the time distortions associated with the shot, as discussed above. Such preconditioned data better comply with the assumption that receiver- and shot-associated contributions to the time distortions are independent. This parallels to some extent what is done in practice when normal-moveout (NMO) correction is applied to data prior to the estimation of residual-static corrections.

Differences such as those in Figure 17 are computed for all source-to-receiver offsets between 0 and X_{max}. The rms average of such differences over the length of the spread provides an overall measure of the departure of the time distortions from those that would be estimated under the assumption of surface consistency. Repetition of this averaging operation for a realistic range of spreadlengths X_{max} yields, as a function of spreadlength, the magnitude of the errors we attribute to failure of the assumption of surface consistency. Figures 18 through 23 show error-estimation curves, computed in this way, for experiments involving different choices of parameters for the near-surface model. The "relative rms error" plotted in Figures 18, 20, and 22 is the ratio of the computed rms-average difference to half the peak-to-trough amplitude of

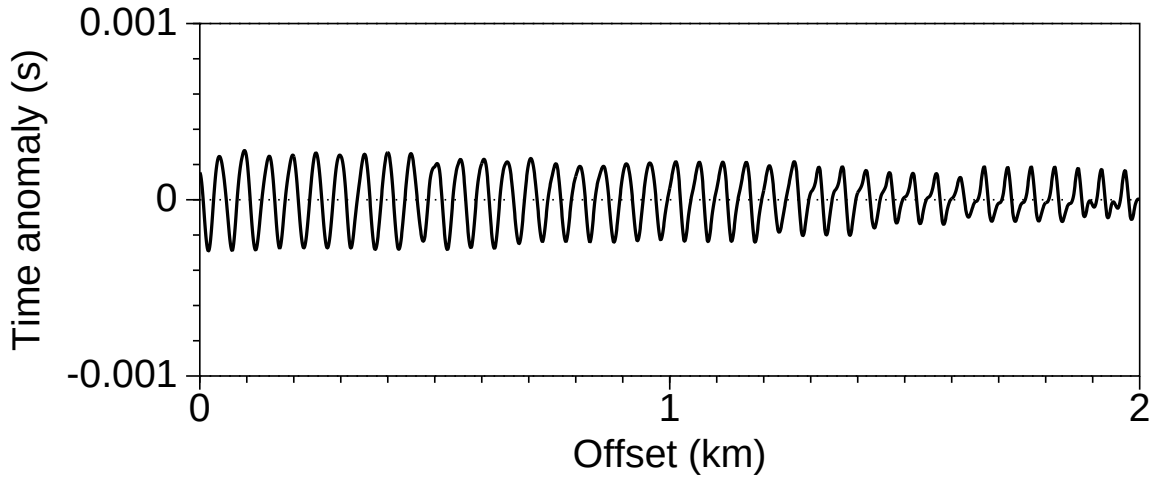

FIG. 17. Difference between the modified time distortions and the estimated surface-consistent reference curves shown in Figure 16. The differences here represent contributions to shortcomings in the surface-consistency assumption for the 50/25/2.5 model with a spreadlength of 2.0 km.

the modified time distortions near zero-offset.

Discussion: the relationship between departure from surface consistency and model parameters

Figure 18 shows error-estimation curves for four choices of the wavelength D of the sinusoidal base-of-weathering. The magnitude of the errors for the larger values ($D = 400$ m and $D = 200$ m) is relatively small, increasing considerably as D is reduced to 100 m, but only for spreadlengths that are larger than those in common practice (i.e., those with $X_{max}/Z > 1$, where Z is the reflector depth). The errors are greatest when D is further reduced to 50 m, reaching relatively large values even for small offsets, i.e., those for which $X_{max}/Z < 1$.

The offset-dependence of the magnitude and phase for the wave-theoretic time distortions is greatest for small D, thus yielding a large departure from the laterally invariant behavior we associate with surface consistency, and, consequently, large relative rms errors, such as those for $D = 50$ m in Figure 18. As discussed in detail in Perez (1997), the variations in the *magnitude* of the distortions are due to wavefront healing while those in the *phase* of the distortions (as observed in Figures 8 and 9) are essentially a ray-theoretical phenomena. Because of Snell's law, raypaths in the near-surface not only depart from vertical, but do so in an offset-dependent manner. The consequent variation in phase of the time distortions is determined by factors such as the thickness of the weathering z_w, the velocity contrast V_1/V_2, and the shape of the base-of-weathering. For example, one should expect more rapid variation in the phase of the distortions with offset for thick than for thin weathering layer because of the increased length of the slant raypath. Thus, the slant-path behavior of wave propagation in the weathering influences the character of the time distortions for both

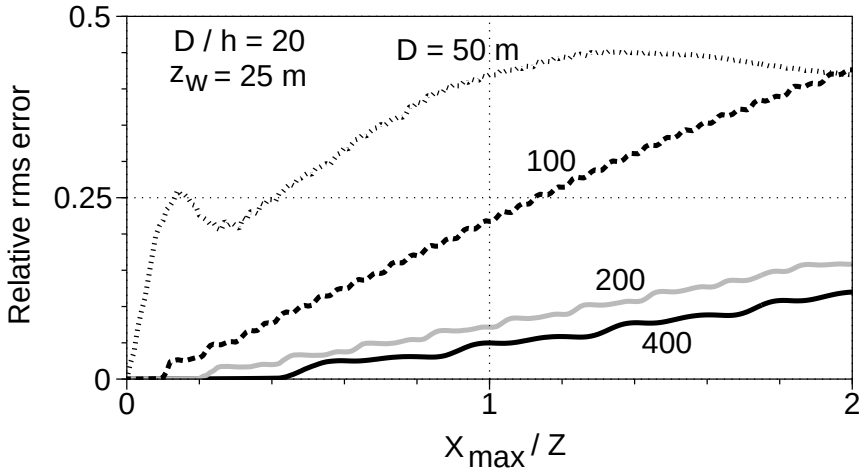

FIG. 18. Error-estimation curves (estimates of the relative error in the surface-consistency assumption) as a function of spreadlength for experiments with values of D ranging from 400 m to 50 m, keeping $D/h = 20$ and $z_w = 25$ m. Spreadlengths X_{max} have been normalized by the depth Z of the reflector, and the computed values of departure from surface consistency have been normalized by half the peak-to-trough amplitude of the time distortions near zero-offset.

long- and short-wavelength anomalies. For larger D, the influence is seen primarily as a moderate increase of the magnitude of the distortions with increasing offset. For smaller D, the major influence is in the increased variation in phase of the distortions; as the weathering thickness increases, the most rapid change in the phase of the distortions occurs for short offsets.

Normalization of the errors by the magnitude of the time distortions, as in Figure 18, gives information on the size of those errors compared to that of the time distortions present in the data, thus indicating to what extent a surface-consistent static correction fails to cure the problem of the time distortions. Since, due to wavefront healing, the magnitude of the time distortions is relatively small for the smaller values of D, this interpretation for the errors in Figure 18 might be pessimistic; the offset-dependent error for $D = 50$ m in Figure 18 is large relative to the time distortions themselves, but those distortions are relatively small. For small D, it may instead be more appropriate to consider a normalization of the errors by the magnitude of the statics computed assuming vertical-ray propagation through the near-surface velocity model.

Such a normalization has been done in Figure 19, for the same models as those in Figure 18 (note that, in Figure 19 and similar figures presented below, we have labeled the errors normalized in this way as "static-normalized rms errors"). For example, the error values for the curve corresponding to the 50/25/2.5 model in Figure 19 have been normalized by half the peak-to-trough amplitude of the *vertical* statics shown by the dotted line in Figure 7.

Since the two different choices for normalization — time distortions near zero-

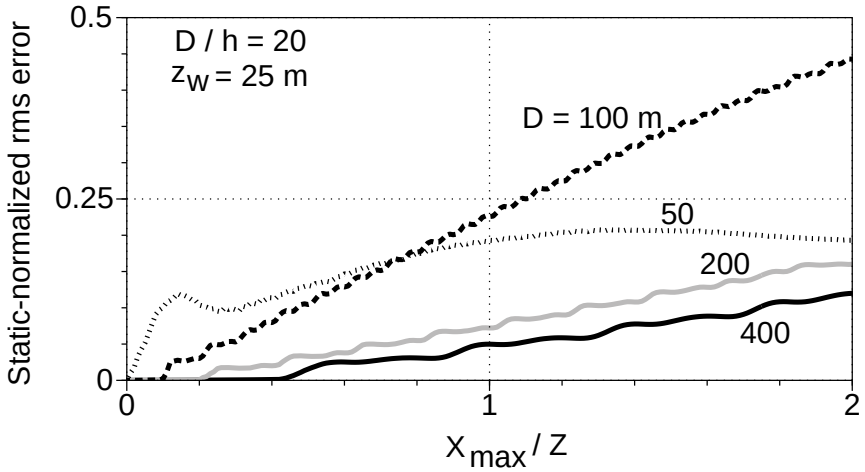

FIG. 19. Error-estimation curves as a function of spreadlength for the same experiments as those whose results are shown in Figure 18. Here, however, the time-distortion values have been normalized by half the peak-to-trough amplitude of the vertical-path statics.

offset and the vertical-path statics — are of similar magnitude for the larger values of D, the corresponding curves (i.e., those for $D = 100$ m and larger) are similar in Figures 19 and 18. The situation is different, however, for $D = 50$ m, since in that case the magnitude of the time distortions is much smaller than that of the vertical-path statics because of wavefront healing. As a result, the errors for $D = 50$ m portrayed in Figure 19 are much smaller than those shown in Figure 18. Moreover, the errors for $D = 50$ m in Figure 19 are generally smaller than those for $D = 100$ m in that same figure. This contrasts with the situation for the relative rms errors shown in Figure 18, which are largest for $D = 50$ m.

For situations in which wavefront-healing causes a reduction in the magnitude of the time distortions, normalization of the errors relative to the vertical-path statics indicates how large are those errors compared to what, hypothetically, would be the size of the time-distortion problem in the absence of wave-theoretical wavefront healing. Because of wavefront-healing, even if the size of the rms errors relative to the magnitude of the time distortions is large, the time distortions, and hence the errors, are small relative to the vertical-path statics. They are also small relative to the time distortions (and the errors) that occur for models in which wavefront healing is of less importance, such as those with larger values of D.

Figure 20 shows the relative rms error estimates for models with a small $D = 50$ m, and variations in the thickness-of-weathering z_w from 10 m to 100 m; h has been kept fixed at a value of 5 m. Here, as in Figure 18 the errors have been normalized relative to the magnitude of the time distortions near zero-offset. The magnitude of the errors increases with increasing depth z_w for $X_{max}/Z < 1.2$; for larger values of X_{max}, the magnitude of the errors reduces somewhat for the large, as compared to intermediate, values of z_w ($z_w = 100$ m compared to $z_w = 50$ m). The magnitudes of the errors

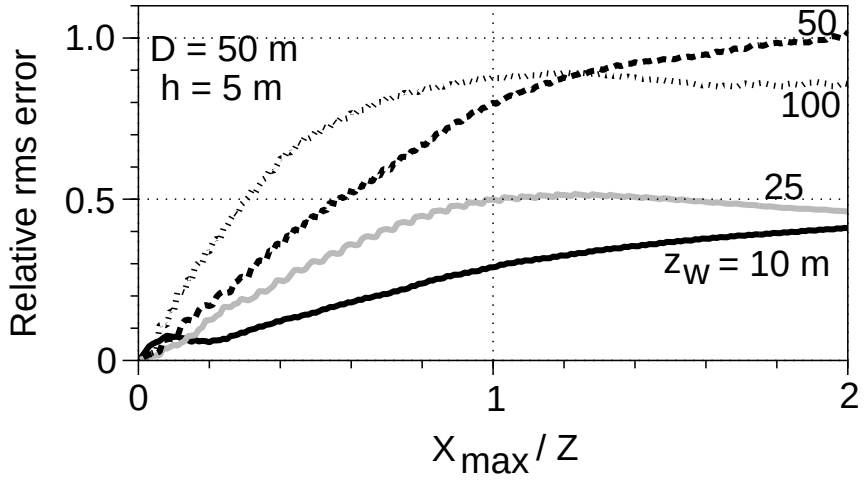

FIG. 20. Curves of the error associated with the surface-consistency assumption for experiments with four different values of z_w, with fixed $D = 50$ m and $h = 5$ m. The errors have been normalized relative to the magnitude of the time distortions near zero-offset, as in Figure 18.

are larger in general in Figure 20 than in Figure 18. Relative errors of a magnitude approaching 1, as observed for some of the models in Figure 20, mean that static corrections under the assumption of surface consistency *fail completely* to solve the problem of time distortions present in the data.

Figure 21 shows the errors for the same models as in Figure 20, this time with normalization relative to the magnitude of the corresponding vertical-path statics. Since wavefront healing is present in the time distortions in all the models considered here ($D = 50$ m in all cases), the time distortions are in general smaller than the vertical-path statics. As a result, the numerical values of the relative errors in Figure 21 are smaller in general than those in Figure 20. As previously discussed, for small values in wavelength D of the base-of-weathering, the variation with offset of the time distortions conforms well to the assumption of surface consistency for the thin-weathering case even though the mollifying action of wavefront healing is limited. For large z_w, the departure from surface consistency is large, corresponding primarily to large variations with offset in the phase of the time distortions (due to departure from vertical raypaths in the weathering layer).

High-velocity near-surface layer.—Regarding the ratio of the velocity of the weathering layer to that in the subweathering (V_1/V_2), the conventional wisdom is that we should expect more severe shortcomings in the assumption of surface consistency as the velocity of the weathering-layer increases relative to that in the subweathering, such as in areas of permafrost: the higher the ratio V_1/V_2, the larger the increase in the magnitude of the time distortions with increasing offset, due to greater departure from the vertical of the raypaths in the weathering. The results of experiments with differing choices of the velocity in the weathering layer V_1, presented in Figures 22

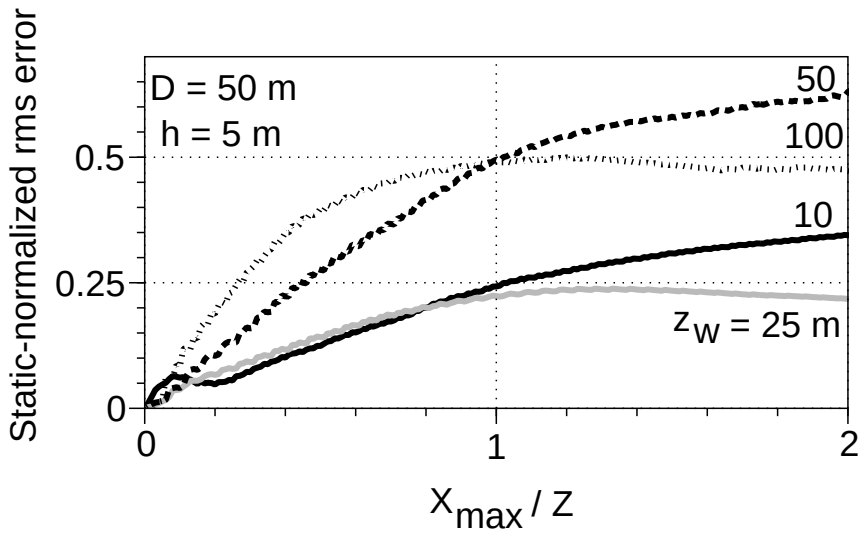

FIG. 21. Error-estimation curves for the same models as in Figure 20, but with normalization relative to the magnitude of the corresponding vertical-path statics.

and 23, however, show what may be surprising behavior. In these figures, V_1 takes values between 1000 m/s and 3000 m/s, with other parameters set at $D = 100$ m, $z_w = 25$ m, $h = 10$ m, and $V_2 = 2000$ m/s. Note, in Figure 22, that a moderate increase in the velocity of the weathering layer V_1 from 1000 m/s to 1500 m/s does lead to an increase in the estimated error, as expected. This trend, however, is reversed for a large increase in the magnitude of V_1. Beyond about $X_{max}/Z = 0.8$, the error for $V_1 = 3000$ m/s *decreases* relative to that for the smaller $V_1 = 1500$ m/s, though it remains slightly larger than that for $V_1 = 1000$ m/s.

Again, Figure 23 presents the results for the experiments with variation in V_1, this time with normalization relative to the magnitude of the vertical-path statics. Figures 22 and 23 are similar in character and in their range of error values, since, in general, the reduction in the wave-theoretic time distortions is small for the models considered here. That reduction, however, is relatively larger for $V_1 = 3000$ m/s than when the near-surface velocity is lower. As a result, the errors shown in Figure 23 are not significantly larger for models with larger ratio V_1/V_2.

The surprisingly small relative errors for $V_1 = 3000$ m/s (for which $V_1/V_2 = 1.5$!) can be attributed to increased wavefront healing of time distortions for larger values of V_1, which in turn can be attributed to the longer seismic wavelength in the higher-velocity weathering layer. The balance between ray bending and wavefront healing yields an overall mild increase in the size of the distortions with increasing offset, resulting in errors for $V_1 = 3000$ m/s that are not as large as might have been expected.

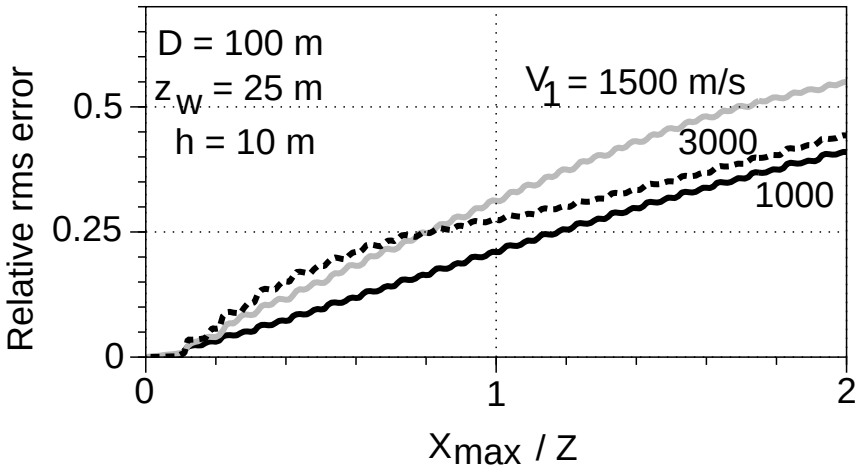

FIG. 22. Errors associated with the surface-consistency assumption for models with differing velocity V_1 in the weathering layer. The subweathering velocity $V_2 = 2000$ m/s in all cases. The error values are normalized relative to the magnitude of the time distortions near zero-offset, as in Figure 18.

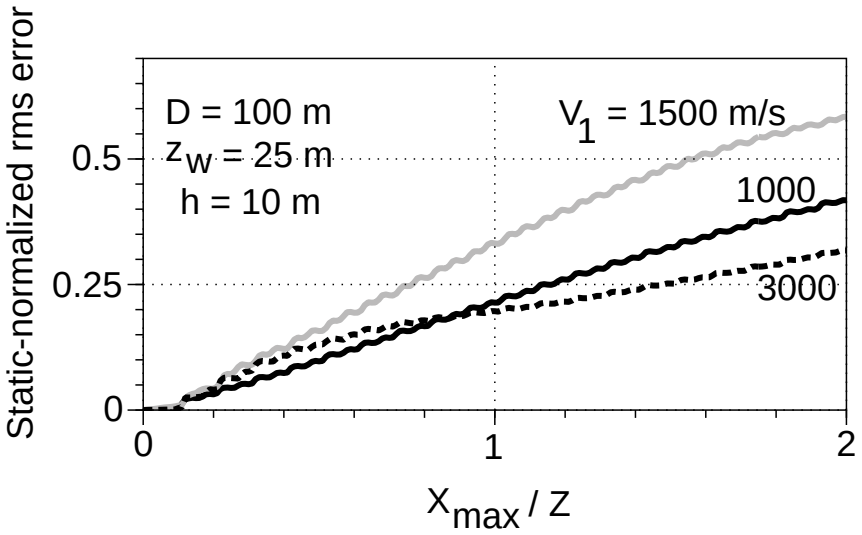

FIG. 23. Error-estimation curves for the same models as in Figure 22, but with normalization relative to the magnitude of the corresponding vertical-path statics.

DISCUSSION AND CONCLUSIONS

Two things that we know for certain about the Earth's near-surface weathering layer are (1) it is complicated and not easily characterized in any particular instance or generalized from any number of such instances, and (2) it does not consist of a homogeneous isotropic layer over a sinusoidal base. Our hope in doing these studies with such simplistic models was that we nevertheless could draw some general inferences about the validity of the assumption of surface consistency (which is at the heart of residual statics-estimation methods) as a function of the depth and scale of anomalies in the weathering layer.

Not only was the subsurface model used in this study simplistic, so were the tests themselves. We have drawn the conclusions, below, from time distortions measured on individual, modeled shot records. Judging that only finite-difference modeling has sufficient modeling accuracy for scattering from small-scale features in the near-surface, and being confronted with the high computation cost of such finite-difference modeling, we could not envisage a modeling study that entailed generation of common-midpoint (CMP) data over enough different models (whether they be "realistic" — whatever that means — or simplistic, such as here) to yield useful conclusions. In working with individual shot records, we have concentrated analysis on receiver-associated statics, arguing that the "drift" in the measured time distortions was associated with the shot and could be removed, under the assumption that shot and receiver statics are independent of one another.

Residual-statics estimation under the assumption of surface consistency is a linear problem, subject to eigenvector-eigenvalue analysis. Unfortunately, the same does not hold for the surface-consistency assumption itself. Nevertheless, through use of models with sinusoidal base-of-weathering, we found characteristics of wave-theoretic time distortions that could be understood as being approximately linear. For example, to an extent, the amplitude of the offset-dependent time distortions due to sinusoidal base-of-weathering is an understandable function of the wavelength of the sinusoid relative to a defined width of Fresnel zone. Two sources of error in our estimates of time distortion — (1) the presence of diffraction and scattering off the weathering base when the wavelength of its sinusoidal variation is short, and (2) dispersion and inaccuracies in (finite-cost) finite-difference modeling for such short-wavelength variations — were major causes of complication in our results that confounded attempts to learn just how useful a linearity assumption might be.

Simple as our models may be, we can surmise from the studies that surface consistency holds best for relatively shallow, relatively long-wavelength anomalies, and, although it may fail for deeper, longer-wavelength anomalies, the healing of wavefronts has the action of reducing the magnitude of statics from such anomalies, making them a less important problem for residual-statics estimation. (In drawing these conclusions, we have loosely associated the depth of the sinusoidal base-of-weathering in our models with the depth of a general anomaly in the Earth's near-surface, and the wavelength D of the sinusoid with the size of the anomaly.)

Two sources of shortcomings in the surface-consistency assumption are (1) that assumption is based on ray theory, and, moreover, (2) all rays are assumed to be vertical in the weathered layer. Being a simplistic ray theory, the reflection-arrival time at each receiver is governed solely by the pencil-thin raypath that crosses the base of weathering. Actual arrivals are waves that are influenced by a zone of some width (the Fresnel zone, or "contributing zone," coined here), and arrival times and locations actually depend on slant-paths through the weathering. Each of these two assumptions gives rise to a different characteristic shortcoming in the surface-consistency assumption.

For many decades, residual-statics estimation has been a highly effective, workhorse tool in compensating for near-surface time distortions in reflection data acquired on land (and offshore as well). It would be surprising to learn, after all, that the assumption of surface consistency doesn't work. Our studies show that, although surface consistency does not hold strictly, it does "work." The assumption, while not valid, is acceptable for practice. Based on our studies, we expect it to hold best for situations in which near-surface time distortions are largest (e.g., where weathering anomalies are either not of small scale or are not deep), and to be most weak where the time distortions are not large (e.g., for deeper anomalies of small scale).

Perhaps surprising, we find that the assumption of surface consistency does not fail so seriously as one might expect when the usual assumption of low weathering velocity is violated, such as in permafrost areas. What helps in such situations is the larger wavefront healing associated with the longer seismic wavelengths in surface layers whose velocity is higher than that of layers beneath. Thus, the departure from vertical paths in such media is compensated to an extent by the increased wavefront healing.

ACKNOWLEDGMENTS

We are grateful to the members of the S(tatics)-team of the Center for Wave Phenomena (CWP) at Colorado School of Mines for helpful discussions. This research was partially supported by the industry sponsors of the Consortium Project on Seismic Inverse Methods for Complex Structures at CWP, the Advanced Computational Technology Initiative of the U.S. Department of Energy, and the National Science Foundation. Support for the graduate studies for Gabriel Perez was provided by Ecopetrol.

References

Alford, R. M., Kelly, K. R., & Boore, D. M. 1974. Accuracy of finite-difference modeling of the acoustic wave equation. *Geophysics*, **39**(6), 834–842.

Berkhout, A. J. 1984. *Seismic resolution: resolving power of acoustical echo techniques*. Geophysical Press.

Bleistein, N. 1984. *Mathematical methods for wave phenomena.* New York: Academic Press.

Cerveny, V., & Soares, J. E. P. 1992. Fresnel volume ray tracing. *Geophysics*, **57**(7), 902–915.

Clayton, R. W., & Engquist, B. 1977. Absorbing boundary conditions for acoustic and elastic wave equations. *Bulletin of the Seismological Society of America*, **67**(6), 1529–1540.

Combee, L. 1994. Wavefield scattering by a 2-D near-surface elliptic anomaly. *Pages 1306–1309 of: 64th Annual Internat. Mtg., Soc. Expl. Geophys., Expanded Abstracts*, vol. 94.

Combee, Leendert. 1995. Scattering of the source-generated wavefield by a 2-D near-surface elliptic anomaly. *Pages 1325–1328 of: 65th Annual Internat. Mtg., Soc. Expl. Geophys., Expanded Abstracts*, vol. 95.

Fei, Tong, & Larner, Ken. 1995. Elimination of numerical dispersion in finite-difference modeling and migration by flux-corrected transport. *Geophysics*, **60**(6), 1830–1842.

Hileman, J. A., Embree, P., & Pflueger, J. C. 1968. Automated static corrections. *Geophys. Prosp.*, **16**(3), 326–358.

Larner, K., Perez, G., Jenner, E., & Salinas, T. 1996. The quality of the surface-consistency assumption in residual-statics estimation. *Pages 1646–1649 of: 66th Annual Internat. Mtg., Soc. Expl. Geophys., Expanded Abstracts.*

Marsden, D. 1993a. Static corrections-a review, Part 1. *The Leading Edge*, **12**(1), 43–49.

Marsden, D. 1993b. Static corrections-a review, Part 2. *The Leading Edge*, **12**(2), 115–120.

Muir, F., Dellinger, J., Etgen, J., & Nichols, D. 1992. Modeling elastic fields across irregular boundaries (short note). *Geophysics*, **57**(9), 1189–1193.

Perez, Gabriel. 1997. *The quality of the surface-consistency assumption in residual statics estimation.* M.Sc. Thesis. Colorado School of Mines.

Sheriff, R. E. 1980. Nomogram for Fresnel-zone calculation (short note). *Geophysics*, **45**(5), 968–972.

Snieder, Roel, & Lomax, Anthony. 1996. Wavefield smoothing and the effect of rough velocity perturbations on arrival times and amplitudes. *Geophys. J. Int.*, **125**, 796–812.

Taner, M. Turhan, Koehler, F., & Alhilali, K. A. 1974. Estimation and correction of near-surface time anomalies. *Geophysics*, **39**(4), 441–463.

Taner, M. Turhan, Wagner, Donald E., Lu, Lee, & Baysal, Edip. 1998. A unified method for 2-D and 3-D refraction statics. *Geophysics*, **63**(1), 260–274.

Vasco, Don W., Peterson, John E., Jr., & Majer, Ernest L. 1995. Beyond ray tomography: Wavepaths and Fresnel volumes. *Geophysics*, **60**(6), 1790–1804.

Wiggins, R. A., Larner, K. L., & Wisecup, R. D. 1976. Residual statics analysis as a general linear inverse problem. *Geophysics*, **41**, 922–938.

Yilmaz, Ozdogan. 1988. *Seismic Data Processing; Investigations in Geophysics 2.* Society of Exploration Geophysicists.